Biochimica et Biophysica Acta, 557 (1979) 265—282

BBA 78544

CORRELATIVE STATISTICAL ANALYSIS AND COMPUTER MODELLING OF INTRAMEMBRANEOUS PARTICLE DISTRIBUTIONS IN HUMAN ERYTHROCYTE MEMBRANES

R.P. PEARSON, S.W. HUI * and T.P. STEWART

Biophysics Department, Roswell Park Memorial Institute, Buffalo, NY 14263 (U.S.A.)

(Received April 26th, 1979)

Key words: Particle distribution; Statistical analysis; Erythrocyte membrane; Computer modeling; (Freeze fracture)

Summary

The planar distribution of intramembranous particles on the P faces of freeze-fractured human erythrocyte membranes is characterized by radial distribution, angular distribution and differential density distribution analysis. Various degrees of intramembranous particle aggregation induced by spectrin removal and low pH are differentiated through computation. Random hard disk models with various disk diameters are built for comparison studies. In all samples, the 80 ± 10 Å particles are found to have a preferred neighboring distance of 100 ± 10 Å, but no preferred angular relation is found between neighboring particles. A pattern recognition process using both radial and density distribution analyses reveals that none of the particle distributions observed may be regarded as random. The fact that the particle distributions observed are neither even nor random suggests that factors other than long range electrostatic force alone are involved in determining the particle distribution.

Introduction

The observation of intramembraneous particles in freeze-fracture faces of biomembranes has created new dimensions in the study of molecular organization of membranes. These intramembraneous particles are generally believed to represent intrinsic protein or complexes formed by protein and lipid molecules. These intramembraneous particles have been observed to translocate laterally on the plane of the membrane as a consequence of various physical-chemical treatments of the membrane, such as: temperature changes [1,2], pH [3,4],

* To whom correspondence and reprint requests should be addressed.
Abbreviations: RDF, radial distribution function; ADF, angular distribution function; DDF, density distribution function.

cation concentration [5], light excitation [6] and certain drug treatments [7]. The movement of these particles indicates that their components are embedded in a fluid environment, as predicted by the 'fluid mosaic model' [8].

Many factors have been postulated to contribute to the forces involved in this particle movement. Lipid domain formation and the consequent partitioning of the protein in these domains has been shown to be the cause for intramembraneous particle patching in some model membranes [9]. This mechanism was postulated to explain similar patching in the plasma membranes of *Tetrahymena* [2], *Acholeplasma laidlawii* [10], and in mitochondrial membranes [11]. Electrostatic interaction between protein molecules has been suggested as one of the intramembraneous particle aggregation forces in erythrocyte ghost membranes [3]. The aggregation of intramembraneous particles in human erythrocytes has also been linked to spectrin disruption and precipitation [4]. In nucleated cells it is likely that microtubules and microfilaments are involved [5,7]. Even though the molecular mechanism involved in particle aggregation is not yet completely understood, the degree of aggregation has been used to differentiate neoplasticly transformed cells from normal cells [12–15], and differences in particle distribution observed in vivo have been linked to membrane alterations in urinary bladder cells [7,16].

In view of the increasing interest in intramembraneous particle distributions, it will be helpful to develop some quantitative parameters to describe the spatial distribution of intramembraneous particles so that pictorial results may be compared and interpreted in a more objective manner. These parameters will enable detection of subtle differences in intramembraneous particle distributions. There have been several qualitative grading systems used to describe intramembraneous particle distribution based upon visual inspection [3,4]. These systems are sufficient in cases where differences in the distributions are obvious, but many important features such as: possible particle pairing or grouping, percentage of empty area, degree of randomness, etc., are difficult to visualize. Mathematical analysis, especially with the aid of computers, is necessary in order to provide a rigorous and objective evaluation of the distributions.

The application of statistical methods in analyzing electron micrographs has been known for some time, especially in the field of morphometry. Its applications in studying the planar structure of membranes have only recently been reported [16–19]. A computer modeling of intramembraneous particle distributions has also been made [20]. Many of these attempts at quantitative studies are limited in respect to the choice of parameters, and sample sizes. Also, the inappropriate choice of a random model may lead to inappropriate conclusions about the degree of randomness of the distributions. We wish to present our efforts in extending these known techniques and adding new methods to quantitate the distribution of intramembraneous particles in membranes. We also offer a correlative study between different analytical methods as an initial step in pattern recognition processes. A preliminary report of this work was presented at a meeting of the Biophysical Society [21].

Materials and Procedures

Sample preparation. The protocol for preparation of the various aggregation states of intramembraneous particles follows that reported by Elgsaeter et al.

[4]. Human erythrocyte ghosts were prepared by the method of Dodge et al. [22] from freshly drawn blood. The sample was divided into two aliquots. One aliquot was suspended in 1/15 Dodge phosphate buffer solution (pH 7.6) plus penicillin (100 U/ml), incubated at 37°C for 22 h, and then pelleted at 20 000 × *g* for 20 min. The incubated samples were resuspended either in 20 mosM phosphate buffer solution at pH 5.0 (group III) or in 1/15 Dodge solution at pH 7.6 (group II). The other aliquot was stored in 1/15 Dodge solution (pH 7.6) at 4°C for 24 h (group I). All samples were allowed to stand for 20 min at room temperature and then were centrifuged at 10 000 × *g* for 20 min.

Freeze fracture, electron microscopy and photography. The concentrated ghosts were cryo-protected with 30% glycerol (v/v, with 1/15 Dodge solution) and frozen in melting freon 22. The frozen specimens were freeze-fractured at −115°C in a Polaron E7500 freeze-fracture module at a vacuum of less than $5 \cdot 10^{-7}$ torr produced by a Perkin Elmer Ultek ion pump unit. Replicas were made by evaporation using Pt/C and C electrodes and were cleaned in undiluted Chlorox solution. The replicas were examined in a Siemens 101 electron microscope. Electron micrographs, selected for flat fractured surfaces, were photographically enlarged to a total magnificiation of 300 000. These enlargements contained a sufficient number of particles for statistical analysis (2000/8 inch × 10 inch print) yet allowed high enough resolution so that digitization errors (approximately 0.5 mm) did not mask the effects we wish to observe.

Digitization. The location of each particle was traced onto transparent sheets placed over the photo-enlargements. In an effort to reduce individual bias in particle identification and placement, these tracings were done by one investigator and subsequently veryfied by another. The tracings were placed over the screen of a Tektronix 4081 graphics display terminal and the terminal's cursor was used to transfer particle coordinates to computer storage. Parallax between the investigator's eye, the transparent overlay and the terminal's display screen are the major source of the 0.5 mm resolution reported above.

Model building. Models were constructed using intramembraneous particle coordinates from random numbers generated by the linear congruential method [23]. Several sets of numbers generated by using different coefficients were tested for best-fit to random distributions. RANDU, from IBM's Scientific Subroutine Package was found to provide sufficiently random numbers for our purposes and was used in all model studies presented here. Additional constraints made upon these models were that the particle concentration was fixed (near the mean particle density found in the various membranes examined) and that the particles had a 'hard sphere' diameter. Particle concentrations specified for these models were between 3400/μm^2 and 4800/μm^2, the range of particle concentrations found in our experiments. The 'hard sphere' constraint was implemented by rejecting any particle within the given minimum distance, d_0, of a previously computed particle's position. Minimum diameters of d_0 = 0, 80, 100 and 120 Å were used to demonstrate the effect of the size of the hard disks in the models. A hexagonal close-packed model was also made in order to evaluate programme operation as an extreme of a highly organized system.

Methods for analysis

Statistical analysis was carried out on a UNIVAC 90/60 computer using a virtual memory, multitasking operating system. The computer programme which has been developed uses statistical methods to analyze three different aspects of the particle distribution; the radial distribution function (RDF), the angular distribution function (ADF), and the density distribution function (DDF).

The radial distribution function measures the distribution of interparticle distances. The function represents the neighboring particle density, $\rho_i(r)$, as a function of distance, r, from each particle in succession. The function $\rho(r)$ is usually expressed as the ratio between the observed particle density, $\rho_i(r)$, and the average particle density, ρ_0. Because of mutual exclusion of hard disks within their diameter, d_0, $\rho(r)$ is usually zero at $r < d_0$ if the hard disk model applies. In a totally 'random' distribution of infinitely small particles ($d_0 = 0$), $\rho_i(r) = \rho_0$ everywhere and the RDF equals 1 for all r. Peaks in $\rho(r)$ define preferred 'interaction distance' between these particles, and the height of the peaks will indicate the prevalence of these interactions.

The angular distribution function evaluates the angular relation between each 'origin' particle and its two nearest neighbors, provided that they lie within a designated interaction distance from the origin particles. It is expressed as the frequency, $A(\theta)$, of pairs of nearest neighbors substaining an angle, θ, about the origin particle. The analysis can be extended to include angular relations between these neighbors and the third nearest neighbor. Sometimes this extension is necessary in order to have a large enough population for reasonable statistical analysis. The $A(\theta)$ curve shows a dip at $\theta < 60°$, due to the mutual exclusion of nearest hard disk neighbors within the circle of radius d_0. Peaks in the ADF will indicate that there are preferred angular relationships between two or more particles. Such peaks may be expected to occur in conjunction with peaks in the RDF if these particles are organized to any degree.

The density distribution function is generated by dividing the surface into equal-sized square areas, counting the number of particles (n) in each square, and ranking the squares according to occupancy. The function, $D(n)$, is dependent upon the size of squares, s, and upon the average particle density, ρ_0, of the sample. The function is more meaningful if it is compared with a known reference distribution. This difference function is called the differential density distribution function (ΔDDF). In order to compare the ΔDDF of various average occupancies, $\langle n \rangle = \rho_0 s$, and various total number of squares, $\Sigma D(n)$, the ΔDDF is normalized against these variables. The normalized function uses the ratio $m = n/\langle n \rangle$ as the argument, and the ratio $D(m)/\Sigma D(m)$ as the value. The differential function, $\Delta D(m)$ is then the difference between the normalized experimental function and the reference function.

$$\Delta D_1(m) = D(m)/\Sigma D(m) - D_1(m)/\Sigma D_1(m)$$

Subscript 1 denotes the model DDF values. If the first function represents values, then $\Delta D_1(m)$ gives the deviation of the experimental curve, from this model.

The choice of the size of squares is important in DDF analysis if one wishes to reveal the characteristic features of a distribution. The size of the squares should be chosen to be less than or equal to the typical dimension of the structural features of interest, such as the area of clustering and/or empty space. In cases where only limited data are available, the character of the distribution may also be affected by the choice of origin. For example, consider that there are only a few empty areas which are about the same dimensions as the square used for analysis. A fortuitous choice of origin will cause these areas to be evaluated as empty while other choices of origin may include particle from the edges of the areas. If such is the case, the distribution may be made origin independent by evaluating the DDF several times and shifting the origin for each analysis. The averaging process reduces statistical noise within the distribution by repeated counting, but the means and variances of the averaged distributions differ only slightly from those of 'fixed origin' distributions.

These three functions portray different aspects of intramembraneous particle arrangement. The ADF and the DDF portray the two-dimensional structure of the system while the RDF treats the system as directionally homogeneous and is therefore a one-dimensional function. The RDF is often used to study and characterize interparticle distance in an 'amorphous' system. It is widely used in the study of liquid and gaseous structures [24,25]. Its application to biological structural study has recently been demonstrated by Knox [17] and by Markovics et al. [19]. The ADF shows preferred angular relationships between sample points. It should be useful in describing polymers linked by bonds at fixed angles. This function has been applied to fluid systems [25], but, to our knowledge, never to biological systems. The DDF is employed mainly to depict grouping and patching of sample points. An application in one-dimensional analysis of the distribution of cell surface anionic sites has been reported [26]. Recently, the density distribution method has been applied to study the IgG distribution on lymphoblasts surfaces [18]. Similar techniques have been used to study the intramembraneous particle distribution in the membrane of human urinary bladder carcinoma [16] and in rat hepatoma cell membranes (unpublished results).

Results

Representative fields of the fracture faces from each of the three experimental groups are shown in Fig. 1. The coordinates of the center of each intramembraneous particle were digitized and plotted as planar distribution maps, one of which is shown in Fig. 2a. Similar plots of distribution maps of 'random' models of hard disks of diameter $d_0 = 0$, 80, 100 and 120 Å are shown in Fig. 2b, c, d and e, respectively. The effects of the constraints of fixed diameter of the hard disks are evident from examination of the minimum particle separations in these maps.

Test models

Two extreme models, a $d_0 = 0$ Å and a hexagonal close-packed model, were employed to test the computer programs used for statistical analysis and for

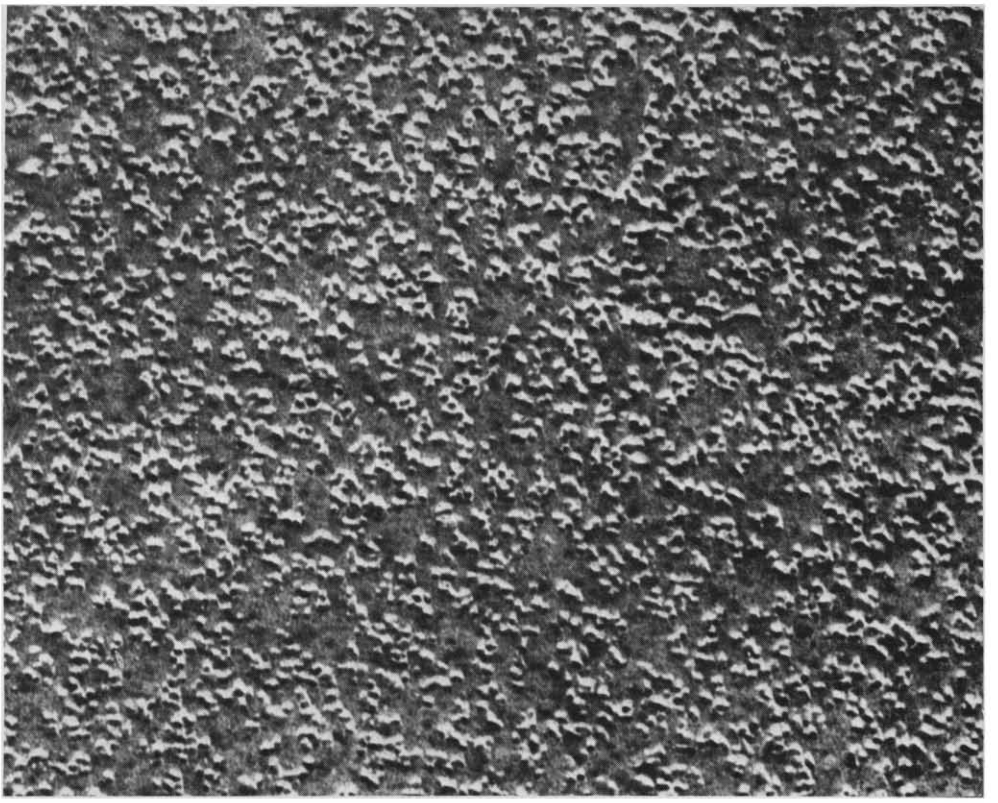

a

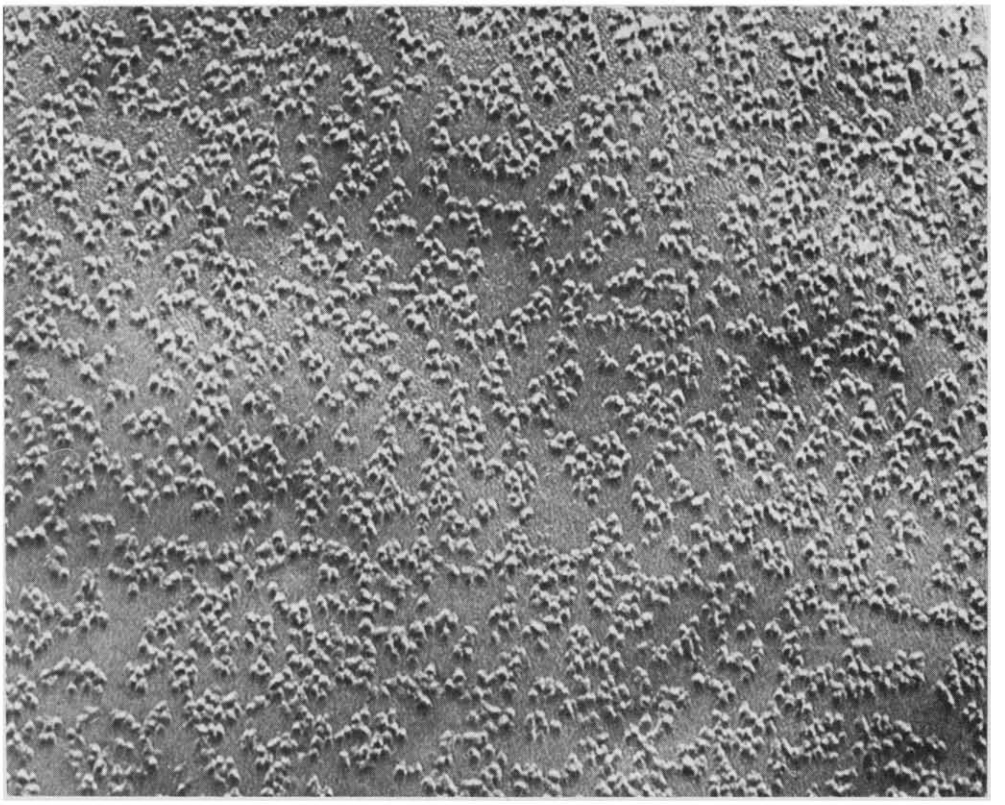

b

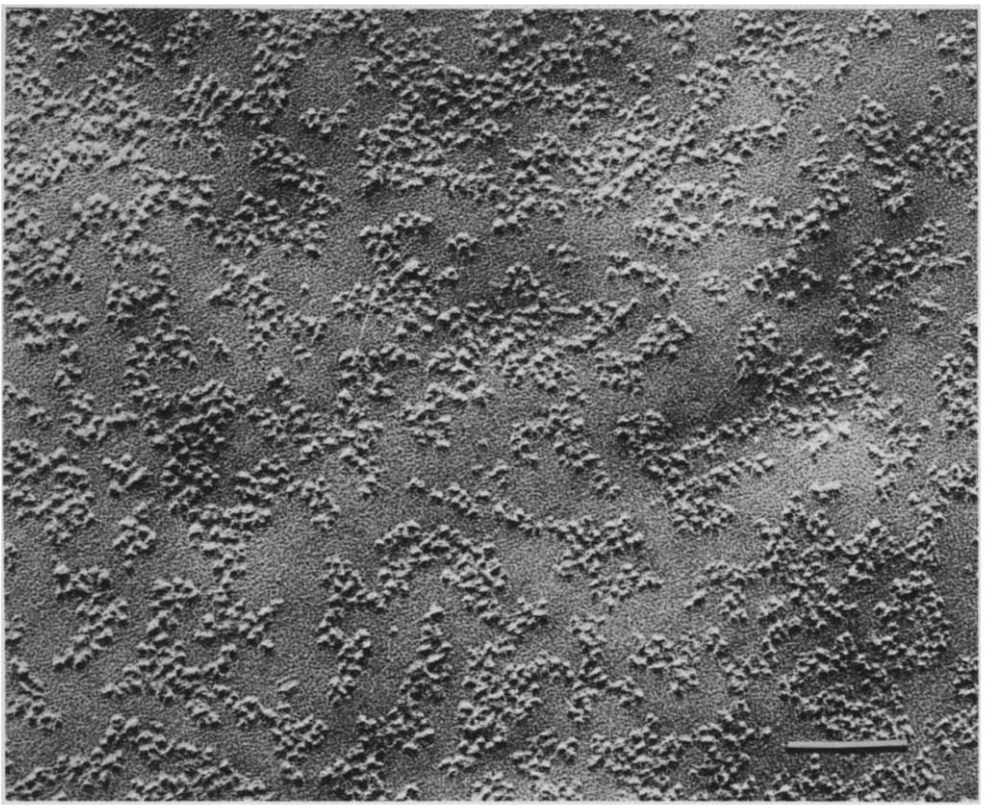

Fig. 1. Electron micrographs of freeze-fracture replicas of P faces of human erythrocyte ghosts. (a) Experimental group I; (b) experimental group II, and (c) experimental group III (bar = 1000 Å).

random number generation. The distribution of more than 4000 numbers generated in each of four runs of RANDU, using different starting numbers for each run, was also examined. The chi-square (χ^2) 'goodness of fit' for the equi-distribution test [23] gave $\chi^2 = 44.4$, 50.3, 55.0 and 42.9. These goodness of fit values lie within the 25—75% probability limits of the χ^2 distribution for $f = 49$. The RDF from each of four runs of the $d_0 = 0$ Å model lies within statistically acceptable probability limits from $\rho(r) = 1$ over the range of inter-particle distances, r, examined. The hexagonal close-packed model presents large, narrow peaks at; $d_0, \sqrt{3}\, d_0, 2\, d_0$, etc., and is zero elsewhere. The DDF for the $d_0 = 0$ Å model follows the Poisson distribution (calculated on the basis of the average particle density and number of grid squares in the model). This result is expected because the model represents a simple random distribution without constraint, and the mean occupancy, $\langle n \rangle$ is small enough (approx. 5) for the Poisson relation to hold. In the opposite extreme, the hexagonal close-packed model distribution is sharply peaked in the interval around the average occupancy value. It does, however, extend into neighboring occupancy intervals because the test grid was not chosen to be an exact multiple of the inter-particle spacing. As with the other distribution functions, the ADF shows its extreme configurations for these two test models. The $d_0 = 0$ Å test model

presents an essentially constant value of $A(\theta) = 1$ while the hexagonal, close-packed model presents sharp peaks at $\theta = 60°$, $120°$ and $180°$. In testing the RDF, ADF and the DDF of the $d_0 = 0$ Å model against those expected from a truely random set of numbers, most of the χ^2 values fall within the 25—75% probability limit and all within the 5—95% limit. It appears that the random number generator is sufficiently random for the purposes of these experiments.

Radial distribution

The RDF curve for the models are presented in Fig. 3 and curves for average

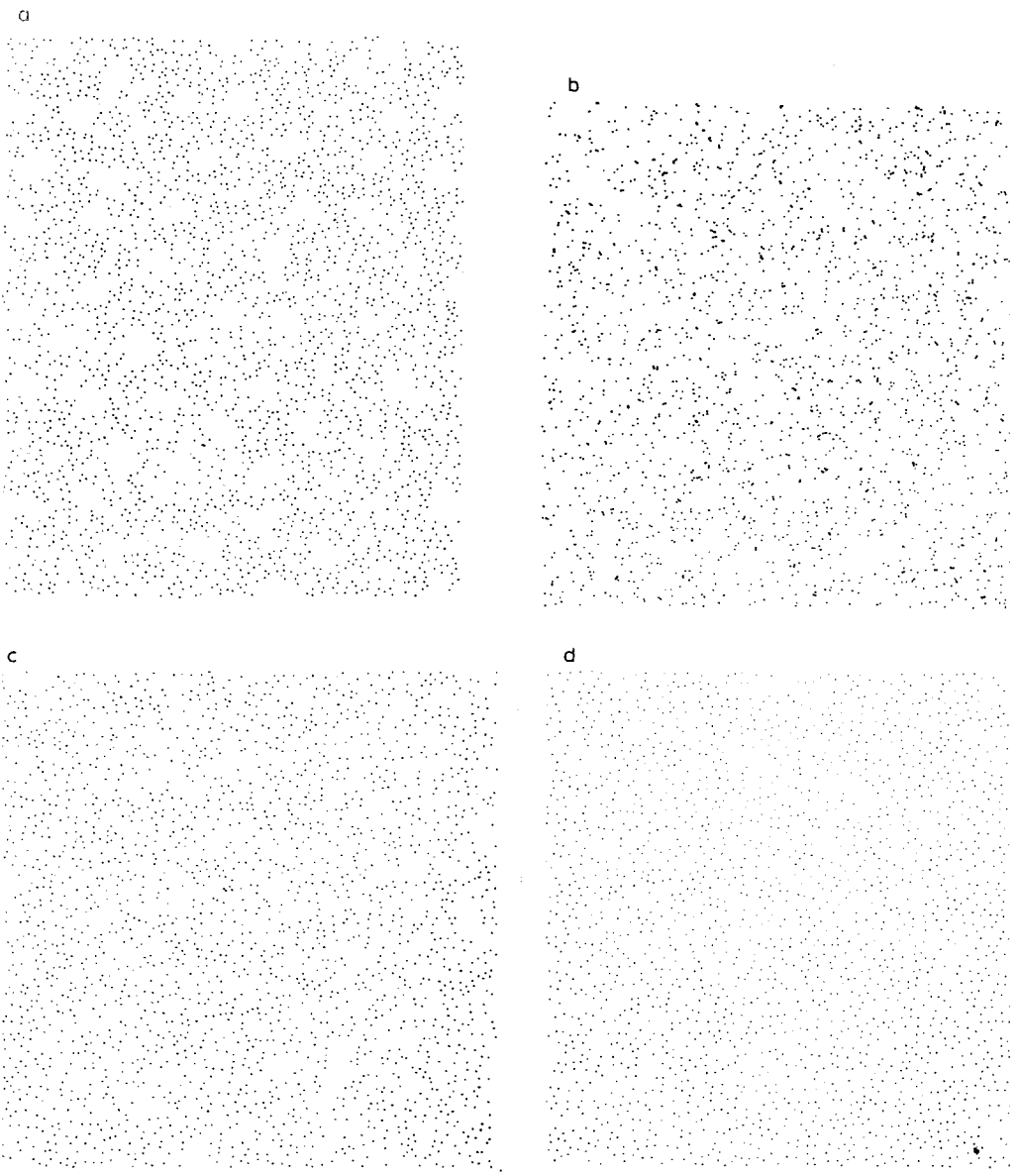

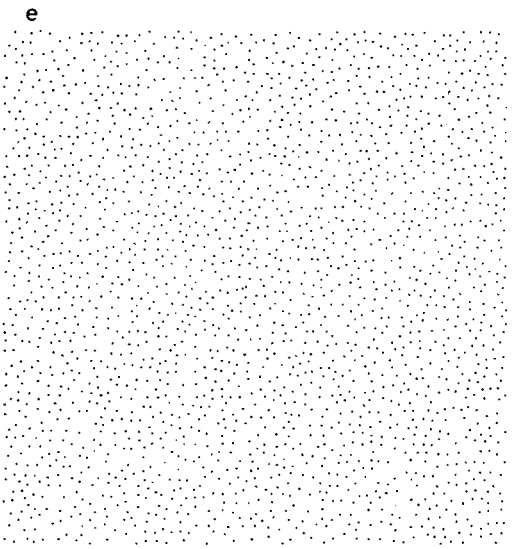

Fig. 2. Position of particles as plotted from coordinates stored in the computer. (a) Pattern from Fig. 1a. (b) Pattern from d_0 = 0 Å model. (c) Pattern from d_0 = 80 Å model. (d) Pattern from d_0 = 100 Å model. (e) Pattern from d_0 = 120 Å model.

RDF values for each experimental group are presented in Fig. 4. The error bars in Fig. 4 show the variations in peak height between samples within each experimental group. The model RDFs show a marked peak which rises abruptly from zero at the 'hard disk' diameter, d_0. This peak is more prominent for larger values of d_0 or for increasing particle densities at the same d_0. This tendency is culminated in the very large peak presented by the hexagonal close-packed model. The experimental groups show a similar increase in peak height in the RDF curves as the particles become more aggregated. The peak heights are listed in Table I. The positions of the peaks are near 100 Å for all experimental groups. If one assumes the limit of resolution in freeze-fracture micrograph to be about 15 Å and the limit of digitization to be also about

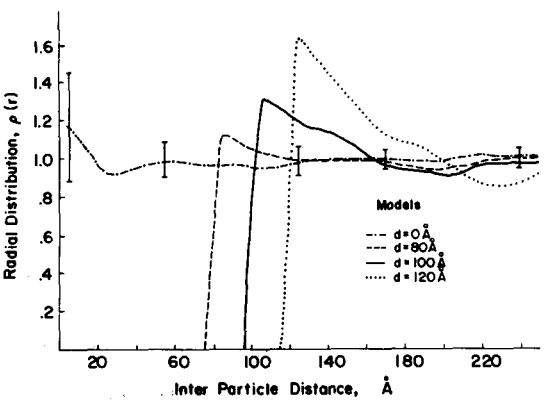

Fig. 3. Radial distribution function for model systems.

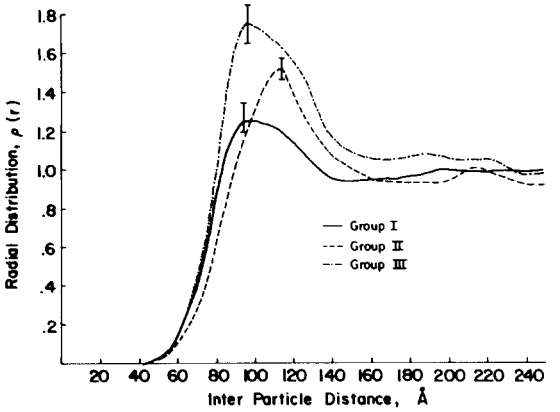

Fig. 4. Averaged radial distribution function for experimental groups I—III.

15 Å, then the peak positions of all samples agree within limits of error. Based on the best fit of peak position, the d_0 = 100 Å model is chosen as the reference model for variance information and ΔDDF distributions (see below).

Density distribution

The histograms representing the DDF for micrographs presented in Fig. 1 are shown in Fig. 5. For comparison purposes, the appropriate curves for the

TABLE I

SUMMARY OF INDIVIDUAL MICROGRAPHS

Aggregation sequence (from visual estimation)	Average of the visual ranking	Experimental group	Particle density (ρ_0)	RDF peak height ($\rho(d_p)^{-1}$)	Total differential ($\int\|\Delta_{100}D(m)\|dm$)
1	1.7	I	3596	0.20	3.8
2	2.2	I	4728	0.34	3.4
3	2.2	I	4440	0.29	3.4
4 [a]	4.5	I	4404	0.34	4.2
5	5.5	II	3887	0.48	6.0
6 [a]	6.7	II	4242	0.50	4.5
7	8.5	III	3499	0.78	8.7
8 [b]	8.5	III	4393	0.86	8.1
9 [a,b]	8.5	III	3700	0.68	8.2
10 [c]	10.0	III	3303	1.05	11.9
0	—	Model	3400	0	7.8
80	—	Model	3400	0.15	2.4
100	—	Model	3400	0.27	0
120	—	Model	3400	0.61	−2.7 [d]

[a] Micrograph is reproduced in Fig. 1.

[b] These samples were printed from different regions of a micrograph of a single cell.

[c] This micrograph shows higher particle aggregation than the average of that group. It was not included in the average curves of Figs. 4, 5 and 7.

[d] The density distribution, $D(n)$, for the d_0 = 120 Å model is narrower and has a higher peak than the reference distribution (d_0 = 100 Å), hence the sense of the integration has been reversed for this model (see also Fig. 8).

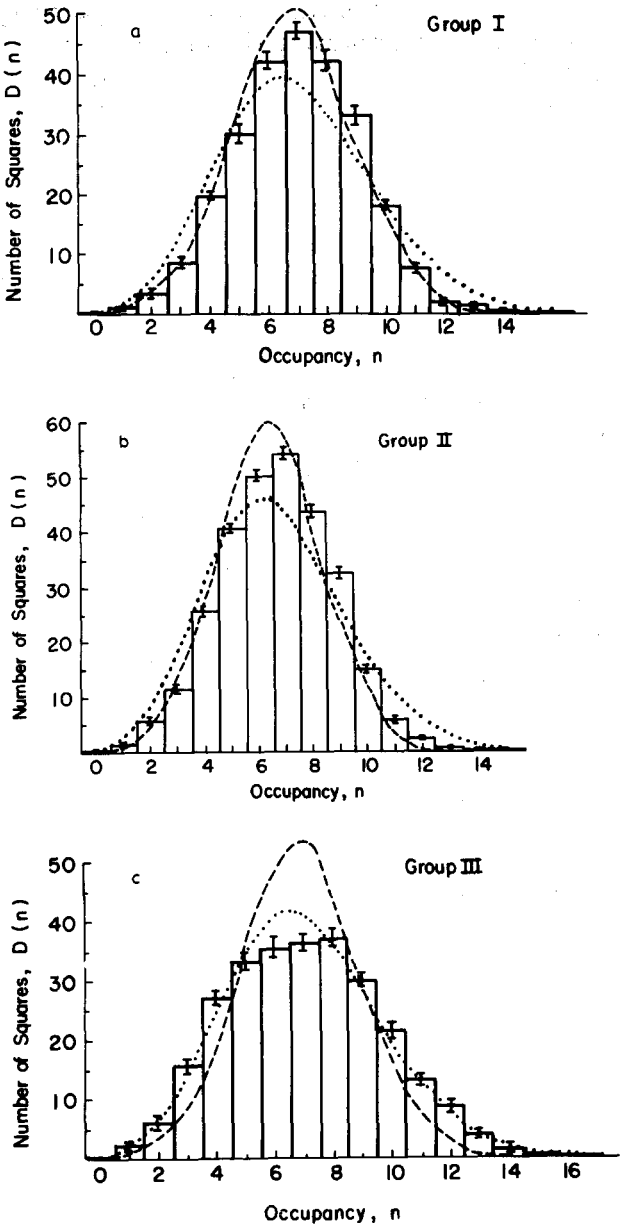

Fig. 5. Histograms showing occupancy of 400 × 400 Å square areas of the surfaces shown in Fig. 1. (a) $D(n)$ from experimental group I (Fig. 1a). (b) $D(n)$ from experimental group II (Fig. 1b). (c) $D(n)$ from experimental group III (Fig. 1c). · · · · · · and - - - - - -, the Poisson and the model d_0 = 100-Å distributions, respectively.

Poisson and $d_0 = 100$ Å (models having the same average particle density and number of grid squares) are superimposed on these histograms. The error bars represent standard deviations estimated for the finite sample size for each interval. Squares of 200 × 200 Å and 400 × 400 Å have been used in this initial analysis. The latter choice improves recognition of the differences between

experimental groups because it approximates better the characteristic patching size of the intramembraneous particles, hence improving the sensitivity of the ΔDDF analysis. The histograms of all samples examined are broader than the $D(n)$ curve of the $d_0 = 100$ Å model. The histograms of group I samples, as represented in Fig. 5a, are closest to the $D(n)$ curve for the $d_0 = 100$ Å model, with histograms from groups II and III samples, respectively, increasingly deviated from it. Relative to the Poisson curve, the $D(n)$ curves for groups I and II are narrower whereas the $D(n)$ curves for group II are broader.

Since the Poisson curves have properties represented by the $d_0 = 0$ Å model (see above) which results in $\rho(r) = 1$ everywhere in RDF analysis and $A(\theta) = 1$ everywhere in ADF analysis, and since these distributions are quite different from corresponding distributions observed in each of our experimental samples, we conclude that the Poisson distribution is not a good model to use for comparison in ΔDDF analysis. Instead, we choose the $d_0 = 100$ Å model as the comparison model because the peak position in RDF analysis as well as other aspects of this model provides the closest approximation to distributions of our experimental samples.

The averages for the $\Delta D_{100}(m)$ for each experimental group are presented in Fig. 6. Error bars show the variations between samples within each experimental group. Since the histograms of the group I micrographs follow the $d_0 = 100$ Å curve closely, the $\Delta D_{100}(m)$ curve deviates the least from zero. The increased broadening of the peaks in $D(n)$ for groups II and III is revealed in the $\Delta D_{100}(m)$ curves of these samples as increased positive deviations at the high and low m values and negative deviations at intermediate m values. These deviations indicate that there are more high and low particle density areas in the micrographs of these experimental groups then there are in the $d_0 = 100$ Å comparison model. In other words, there is increasingly higher particle aggregation in groups II and III. The integrated deviations $\int|\Delta D_{100}(m)|dm$, as listed in Table I, reflect the state of aggregation of each micrograph.

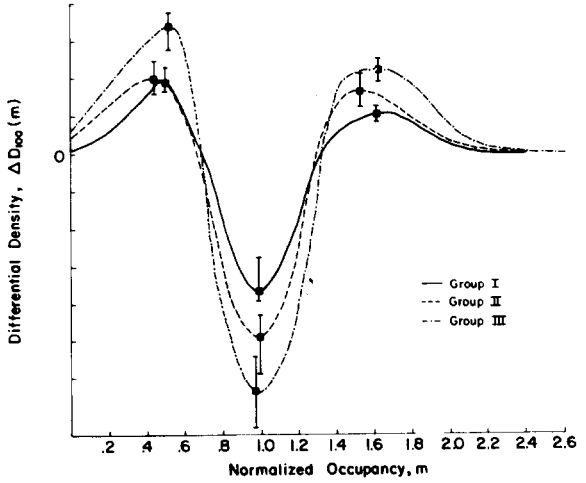

Fig. 6. Averaged differential density distribution for the experimental groups using the $d_0 = 100$ Å comparison model.

Angular distribution

The ADFs of each experimental group are presented in Fig. 7. The error bars in Fig. 7a show the magnitude of the statistical error as described below. The curves show few features above these statistical error limits. The error bars in Fig. 7b show the extremes in variation between samples within each experimental group. In all instances, there appears to be a peak in the distribution near $\theta = 60°$ which is somewhat larger for experimental group III and for the closer packed $d_0 = 120$ Å model than for the other distributions.

Error analysis

Three sources of error must be included in the analysis. (A) Statistical error due to limited number of particles in a sample interval; (B) errors in identifying particles and in correctly assigning coordinates to these particles, and (C) error due to sampling variability in the specimens. We estimated the statistical error by computing three runs of the $d_0 = 100$ Å model distribution and calculating the variance between these runs for each segment of the distribution functions. As expected, the standard deviation in the RDF is larger over the segment $r =$ 100—110 Å than over the segment 200—210 Å (e.g. 0.06 vs. 0.04). This difference occurs because there are fewer particles in the rings of small r. There are fewer particles in each ADF interval than in the RDF intervals, so standard deviations are larger for the ADF (e.g. 0.14). These errors are indicated as error bars in the graphs of the distributions for the models (Figs. 3, 5 and 7a).

Error in identification and in estimation of the coordinates of each particle may be larger than 0.5 mm on the 300 000 × photographic prints we have analyzed. This error corresponds to an uncertainty of 15 Å in the freeze-fracture replicas. However, based on the observation that the position and height of the peaks in the RDF differ by less than 10 Å in two independent tracings of the same micrograph, we conclude that the effect of this error is small when averaged over all particles in a sample.

The error due to sampling variability cannot be easily estimated. We have

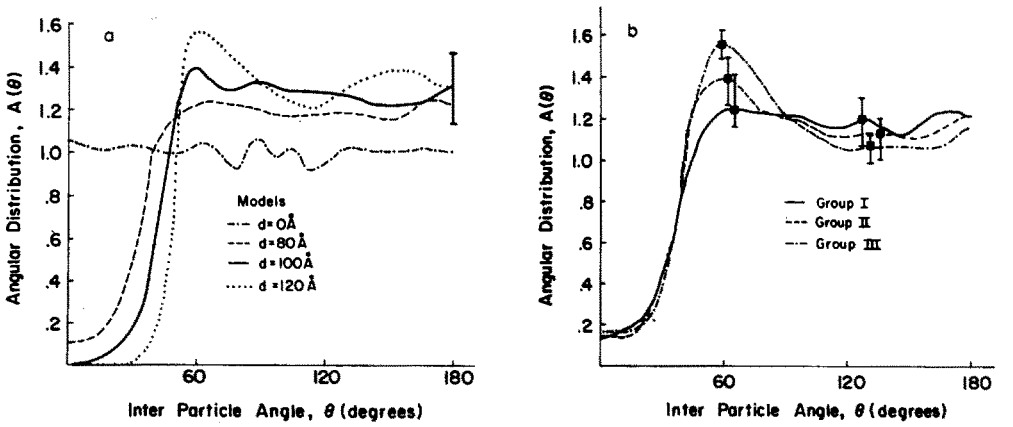

Fig. 7. Averaged angular distribution functions; (a) for the model systems; (b) for the experimental curves.

analyzed at least three micrographs for each experimental group in order to estimate the size of this error and find that it is of about the same magnitude as the statistical errors discussed above. This magnitude is represented as error bars in distributions for the experimental groups (Figs. 4, 6 and 7b).

Visual estimation

Since it is realized that there is considerable variation between samples within an experimental group; a parallel experiment was conducted in which we used visual estimation ranking of the electron micrographs evaluated by the statistical methods described above. Four colleagues were asked to rank the micrographs in order of the aggregation state of the intramembraneous particles. In spite of some variations in particle density, magnification, and contrast in the micrographs, all micrographs of each experimental group were ranked together. However, the most aggregated sample of a group sometimes was ranked closer to the next group than to their own group (Table I, column 2). When the distribution maps (the tracings or the plotted maps) of the micrographs were ranked, however, the experimental groups were no longer separable, especially between groups I and II. The reason for this poor result may have been the lack of additional visual clues, such as particle size or shape. The range of aggregation states is quite small, it is only between states 0—3 of the scale devised by Elgsaeter and Branton [27].

Discussion

This project was initiated in order to develop methods for the objective analysis of intramembraneous particle distributions in biomembranes. In particular, we have been interested in finding any deviation from randomness. In addition to the usual, rather subjective visual ranking technique, we have employed two computational approaches to the problem. First, we used a combination of three statistical functions in order to provide a quantitative description of particle distribution and, secondly, we developed a model system which rather closely approximates the observed intramembraneous particle distributions. This model, the random, hard disk model, is a considerable improvement over the often used Poisson distribution model [16]. An advantage of the present study over many of the previous studies [16,17,20] is that a large number of particles were measured in each sample (1000—2000) which reduces statistical errors.

Characteristics of the distribution analyses

For all experimental RDF curves, the edge of the peak on the small r side of $r = d_p$ (peak distance) is sloped, rather than vertical as in a hard disk model. This indicates either that intramembraneous particles have a single size but that they deform as 'soft' disks, or that intramembraneous particles are rigid but they have a range of sizes. A model incorporating these features would use many arbitrary parameters not directly determinable from our experimental data and is, therefore not pursued in this paper. A closer look at the distribution analysis of the hard disk random model shows that the characteristics of the 'random' distribution depends a great deal on the diameter, d_0, of the

particles and the average particle density, ρ_0, i.e. the fraction of available area occupied by the particle. When $d_0^2\rho_0 << 1$, the chance that two particles are in contact is very small, and the effect of particle size on these distributions is small. In this case, the unconstrained random function, i.e. the Poisson distribution, applies. In our three constrained models of $d_0 = 80$, 100 and 120 Å, the values of $d_0^2\rho_0$ are 0.22, 0.32 and 0.49, respectively. The progressively severer constraint on these models is manifested by increasing peak heights of $\rho(r)$ in RDF analysis. The peak at $r = d_0$ is present also in other formulations of random hard disk models [28,29] and is not a particular feature of our models. The effect of the increasing constraint is also evident in the increasing narrowness of the peak of $D(n)$ in DDF analysis. The effects of d_0^2, ρ_0 on $A(\theta)$ are relatively less extreme.

It should be noted that particle density, ρ_0, varies somewhat in the micrographs we analyzed. The range of ρ_0 is between 3300 and 4700/μm^2, which falls on the wide range of ρ_0 values reported previously for human erythrocyte membranes [20,30] and is typical of the wide range of particle densities observed in other plasma membranes [31]. We have taken care in choosing only the flat portion of the membrane normal to the incident illumination for analysis purposes. The variation may be caused by erroneous identification of intramembraneous particles, by preferential removal of particle-rich or particle-free regions during treatment [4] or by the actual variations within each specimen. As a further check on the reproducibility of our procedures, two regions from an electron micrograph of a single cell were printed, traced, and analyzed. Although ρ_0 and the peaks at $r = d_p$ in $\rho(r)$ were different, the total differential density for these two specimens were almost identical (see Table I, sequence Nos. 8 and 9). The stability is in part due to the normalization procedure against variations in ρ_0 which are used in determining $\Delta D_{100}(m)$.

The $A(\theta)$ of all experimental groups are as featureless as that of the $d_0 = 100$-Å models. The suggestive peak in group III near $\theta = 60°$ is still weaker than that in the $d_0 = 120$ Å model, indicating that there is practically no directional organization of the intramembraneous particles in the membrane. A sometimes illusive impression of reticulated structures in particle distributions, such as those seen in Fig. 2b, are a visual artifact.

Pattern recognition evaluation of randomness

Since both the peak heights of $\rho(r)$ and the integrated ΔDDF values are separate measurements of deviation of a sample from a random model, the relation between the two parameters should give some insight into the nature of the deviation. Fig. 8, a scatter diagram of these two parameters, shows a definite relationship between them. This relationship is independent of the choice of the comparison model for ΔDDF, since a change in model involves only a shift of origin along the ordinate. The slope of the regression line may provide information concerning the de-randomization process. The sample in experimental group II lies in an intermediate region of the graph between experimental groups I and III. Thus we can use this plot as a pattern recognition procedure to separate the various experimental groups. The boundaries between the experimental groups are indicated by dashed lines in Fig. 8.

In our experiment, the most preferred neighboring distance, d_p, as deter-

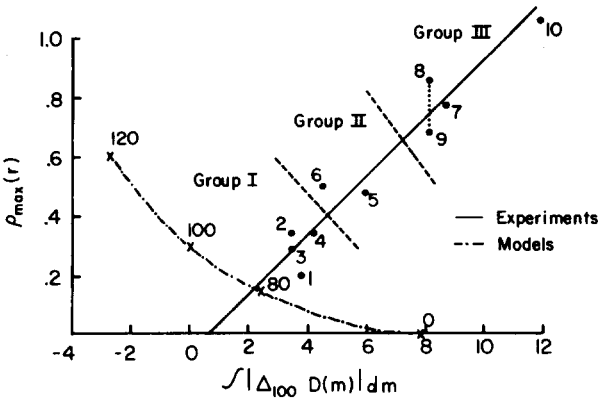

Fig. 8. Scatter diagram showing relationship between RDF maximum peak height at $r = d_p$ and integrated differential distribution function (d_0 = 100 Å comparison mode). X, distribution from models, the numbers indicate value of d_0; ○, experimental samples as numbered in Table I, column 1.

mined from RDF analysis, is 100 Å. However, use of the d_0 = 100 Å model produces significant values for the integrated ΔDDF even for experimental group I data (see Table I, column 6 and Fig. 8).

Given the free choice of d_0 it is usually possible to build a model which closely matches any given experimental $D(n)$. For example, one of our group III distributions may be matched with the $D(n)$ of the d_0 = 0 Å model. Thus ΔDDF analysis alone is meaningless unless d is known from other measurements. Since ρ_0 is determined directly and d_p is chosen from the peak position of experimental $\rho(r)$ curve, the particular hard disk model used for comparison in the $\Delta D(m)$ curves is predetermined by experimental evidence. No adjustable variable is involved and our analysis is therefore quite dependable. This is illustrated in Fig. 8. In order to fit the $\Delta D(m)$ curve well, one requires a model consisting of predominantly d_0 = 80-Å disks. This contradicts the observed peak at 100 Å in $\rho(r)$. Furthermore, according to the regression relation presented in Fig. 8, group I seems to be as close to the limit of randomness allowed since further reduction of the integrated $\Delta D_{100}(m)$ will result in a very low peak height at $r = d_p$ in $\rho(r)$. Such a low peak in $\rho(r)$ is, however, incompatible with the peak height expected for random models. It seems that simultaneously satisfying the RDF and ΔDDF requirements is impossible. Therefore, based on correlation between RDF and ΔDDF analyses, we conclude that the distribution of intramembraneous particles in the membrane of all our sample groups, including the control, is not completely random as sometime speculated [31].

Implications on particle interactions

The specimen preparation procedures in this experiment followed closely to those reported by Elgseater et al. [4]. According to their interpretation, group I membrane is almost intact, group II membrane has lost approximately 70% of its spectrin while the intramembraneous particles are still not aggregated. Group III is an extreme case of particle aggregation caused by the precipitation of the remaining spectrin in the membrane. From our pattern recogni-

tion results, we found some non-randomness in the control group I. Group II had already started to aggregate, although not yet apparent by causal inspection. The removal of spectrin may encourage the intramembraneous particles to move more freely. These particles may then start to aggregate due to protein interaction [4] or preferential association of protein with heterogeneous domains of lipids [9]. Since the particles in the highly aggregated group III sample do not show any directional ordering in our ADF analysis, it is likely that these particles were forced into patches without strong interparticle interactions from specific interaction sites on the particles. The peak heights at $r = d_p$ in $\rho(r)$ for experimental group I is nearly the same as for the $d_0 = 100$ Å model (see Table I). If a repulsive force between intramembraneous particles were to have an appreciable effect, intramembraneous particles would be more evenly distributed than in the hard disk random model, where no long-range forces act. In the extreme case where there is strong long-range forces between intramembraneous particles, the distribution would approach hexagonal packing where each particle is at a maximum distance from every other particle. We observe the opposite effect, i.e. greater aggregation in our experimental groups than in the random model. This observation indicates that there is no appreciable long-range repulsive force such as electrostatic repulsion between particles, as has been suggested [3,4].

The $\rho(r)$ of all experimental samples show a peak at $r = 100$ Å. This common dimension indicates that there is a preferred distance, d_p, between centers of these intramembraneous particles. Analogous to the peak at $r = d_0$ in $\rho(r)$ for the model systems, this peak implies that the majority of particles have a diameter of 100 Å. However, the typical diameter of the intramembraneous particles, as measured directly from our electron micrographs is $80° \pm 10$ Å. Although directly measured particle diameters vary according to replication technique, most of the reported values for human erythrocyte particles are in the range of 85—105 Å [33]. The fact that our values for d_p is at the upper limit rather than in the mid range of the directly measured particle diameters, suggest that the particles are kept apart in some manner. This separation may be caused by the spatial exclusion of the portion of the particles unobservable from the fractured face (i.e. an iceberg effect). Alternatively, the separation may be caused by a short-range, mutually repelling force such as shielded electrostatic force, or by an impenetratable ring of lipid surrounding each particle. The details of this mechanism await further clarification.

Conclusion

Our quantitative analysis may be generalized to study other planar distributions in biomembranes [34]. It provides a comparable and more objective evaluation than visual examination and qualitative grading. These methods are examples rather than exhaustive representation of a variety of mathematical methods which may be applied to study less-ordered molecular assemblies in biological specimens. Since regular biological structures are exceptions rather than rules, these analytical methods are of considerable importance in the structural analysis of biomembranes.

Acknowledgements

We wish to thank Dr. R. Rein of this Institute for the use of his computer graphic facility, supported by a grant from NASA No. NSG-7305-89057-01. This project was supported by a grant from the American Cancer Society BC-248. S.W.H. is a recipient of a Career Development Award from the National Cancer Institute, CA00084.

References

1 Hochli, M. and Hackenbrock, C.R. (1977) J. Cell Biol. 72, 278—291
2 Speth, V. and Wunderlich, F. (1973) Biochim. Biophys. Acta 291, 621—628
3 Pinto de Silva, P. (1972) J. Cell Biol. 53, 777—787
4 Elgsaeter, A., Shotton, D.M. and Branton, D. (1976) Biochim. Biophys. Acta 426, 101—122
5 Volsky, D. and Loyter, A. (1977) Biochim. Biophys. Acta 471, 243—259
6 Staehelin, L.A. (1971) J. Cell Biol. 71, 136—158
7 Wade, J.B., Kachadorian, W.A. and Discala, V.A. (1977) Am. J. Physiol. 232, 77—83
8 Singer, S.J. and Nicolson, G. (1972) Science 175, 720—731
9 Kleeman, W. and McConnell, H.M. (1976) Biochim. Biophys. Acta 419, 206—222
10 Verkleij, A., Ververgaert, P., Van Dennen, L. and Elbers, P. (1972) Biochim. Biophys. Acta 288, 326—332
11 Hackenbrock, C.R., Hochli, M. and Chau, R.M. (1976) Biochim. Biophys. Acta 455, 466—484
12 Torpier, G., Montagnier, L., Biguard, J-M. and Vigier, P. (1975) Proc. Natl. Acad. Sci. U.S. 72, 1695—1698
13 Furcht, L.T. and Scott, R.E. (1975) Exp. Cell Res. 96, 271—282
14 Pinto de Silva, P. and Martinez-Palomo, A. (1975) Proc. Natl. Acad. Sci. U.S. 72, 572—576
15 Gilula, N.B., Eger, R.R. and Fifkin, D.B. (1975) Proc. Natl. Acad. Sci. U.S. 72, 3594—3598
16 Weinstein, R.S. (1976) Cancer Res. 36, 2518—2524
17 Knox, E.G. (1977) Br. J. Haematol. 37, 537—541
18 Abbas, A.K., Ault, K.A., Karnovsky, M.J. and Unanue, E.R. (1975) J. Immunol. 114, 1197—1204
19 Markovics, J., Glass, L. and Maul, G.G. (1974) Exp. Cell Res. 85, 443—451
20 Finegold, L. (1976) Biochim. Biophys. Acta 448, 393—398
21 Pearson, R., Stewart, T. and Hui, S. (1978) Biophys. J. 21, 203a
22 Dodge, J.T., Mitchell, C. and Hanahan, D.J. (1963) Arch. Biochem. Biophys. 100, 119—130
23 Knuth, D.E. (1969) The Art of Computer Programming, Vol. 2, Seminumerical Algorithms, Chapter 3, Addison-Wesley Pub. Co., Inc., Reading, MA
24 Gunier, A. (1963) X-ray Diffraction, p. 55, Freeman, San Francisco
25 Bernal, J.D. (1964) Proc. R. Soc. A 280, 299—322
26 Weiss, L., Jung, O.S. and Ziegel, R. (1972) Int. J. Cancer 9, 48—56
27 Elgsaeter, A. and Branton, D. (1974) J. Cell Biol. 69, 1018—1030
28 Zernicke, F. and Prins, J.A. (1927) Z. Phys. 41, 184
29 Chae, D., Res, F. and Ree, T. (1969) J. Chem. Phys. 50, 1581—1589
30 Bachi, Th., Whiting, K., Tanner, M., Metaxas, M. and Anstee, D. (1977) Biochim. Biophys. Acta 464, 635—639
31 Scott, R. and Marchesi, V. (1972) Cell. Immunol. 3, 301—317
32 Martinez-Palomo, A., Chavez, B., Gonzalez-Robles, A. (1978) In Electron Microscopy 1978, Vol. III, Proceedings of the Ninth Int. Congr. on Electron Microsc. (Sturgess, J.M., ed.), Microsc. Soc. Canada, Toronto, 1978, pp. 503—515
33 Kitajima, Y., Sekiya, T. and Zozawa, Y. (1976) Biochim. Biophys. Acta 445, 453—465
34 Nicolson, G.L. and Painter, R.G. (1973) J. Cell Biol. 59, 395—406